Int. J. Heat Mass Transfer. Vol. 35, No. 11, pp. 2931–2940, 1992
Printed in Great Britain

0017–9310/92 $5.00 + 0.00

Natural convection near a small protrusion on a vertical plate

S. GHOSH MOULIC and L. S. YAO
Department of Mechanical and Aerospace Engineering, Arizona State University, Tempe, AZ 85287-6106, U.S.A.

(*Received* 30 *July* 1991 *and in final form* 30 *November* 1991)

Abstract—Natural convection in the vicinity of a small protrusion embedded in the boundary layer on a vertical flat plate is considered. Protrusions of height $\sim L\varepsilon^{9/7}$ and length $\sim L\varepsilon^{6/7}$, where $\varepsilon = Gr^{-1/4}$, are analyzed in the context of double-deck theory. The lower deck equations are solved numerically by a hybrid spectral finite difference method. The heat transfer rates are determined for two thermal boundary conditions. In the first case, the protrusion is maintained at the same temperature as the plate, while in the second case, the protrusion is held at a temperature higher than the plate temperature. The effect of boundary layer separation on the heat transfer rate is investigated.

1. INTRODUCTION

THIS PAPER is concerned with heat transfer in the vicinity of a small protrusion embedded inside a jet-like boundary layer on a flat plate. This is a model to study the cooling of electronic chips, and also to study the details of flow and heat transfer near a single roughness element on an otherwise smooth plate. The presence of a protrusion can produce significant local changes in the flow along a flat plate and alter the heat transfer rates appreciably. If the size of the protrusion is large, boundary layer separation may occur. The induced mixing due to boundary layer separation may enhance the rate of heat transfer. The natural convection boundary layer along a vertical flat plate has been used as an example of a jet-like boundary layer flow in this paper. The results can be applied to other jet-like boundary layer flows over protrusions where the fluid outside the boundary layer is at rest or moving much slower than the fluid inside the boundary layer such as the wall jet produced by a source of momentum upstream.

The flow over a protrusion embedded in a jet-like boundary layer on a flat plate may be described by a double-deck structure [1–4] if the streamwise length of the protrusion is $O(L\varepsilon^{6/7})$ and its height is $O(L\varepsilon^{9/7})$, where L is the distance from the leading edge of the plate to the location of the protrusion and $\varepsilon = Re^{-1/2}$ or $Gr^{-1/4}$ [5]. Here, Re is the appropriate Reynolds number for forced flows such as the wall jet, and Gr is the Grashof number for natural convection. The double-deck structure follows closely the usual triple-deck ideas for local boundary layer interactions [6–9], the difference being that here there is no outer flow; hence, there is no upper deck. The presence of the protrusion results in large streamwise accelerations and temperature gradients in a small region around the protrusion, and the flow cannot be described by the classical boundary layer equations. In the outer part of the boundary layer, the viscous and the conduction terms do not change significantly from their upstream values, and the perturbed flow is described by inviscid-flow equations. The inviscid perturbations do not satisfy the no-slip and wall temperature boundary conditions. Near the wall, there exists a sublayer or lower deck where the viscous and conduction terms cannot be neglected. Thus, the boundary layer is divided into two parts, an outer layer or main deck, and an inner sublayer or lower deck. The flow in the lower deck is described by the boundary layer equations, but with an induced pressure gradient to account for the presence of the protrusion. The pressure outside the boundary layer being constant, there must exist a transverse pressure gradient across the main deck to sustain the induced streamwise pressure gradient in the lower deck. The double-deck structure provides a consistent description of this viscous–inviscid interaction for a jet-like boundary layer.

The induced pressure gradient may be adverse in some regions, and, if large enough, may trigger off boundary layer separation although there is no external free stream. Due to the quasi-elliptic nature of the double-deck pressure–displacement interaction, the Goldstein singularity, which appears in the classical boundary layer equations at separation, does not occur in the lower deck equations. Thus, small-scale separated flows may be computed numerically using the double-deck model.

The present investigation has been restricted to protrusions which fall into the double-deck scale. The flow over a hump inside a free-convection boundary layer has been analyzed in the context of double-deck theory by Merkin [5]. Merkin, however, did not obtain a solution for the energy equation since temperature perturbations on the double-deck scale do

NOMENCLATURE

a	displacement function
d	displacement function in transformed coordinates
f	surface geometry function
g	gravitational acceleration
Gr	Grashof number
h	height of protrusion
k	thermal conductivity
L	length from leading edge of plate to protrusion
Nu	Nusselt number
p	pressure
Pr	Prandtl number
Q	total heat transfer rate from protrusion
T	temperature
T_0	temperature of surface of protrusion
T_w	plate temperature
T_∞	ambient temperature
u	x-component of velocity
u_0	characteristic velocity
v	y-component of velocity
w	transformed velocity
x	axial coordinate
y	transverse coordinate
z	transformed transverse coordinate.

Greek symbols

α	thermal diffusivity
β	thermal expansivity
γ	$=\int_0^\infty [U_B(t)]^2\,dt$, a constant used in the double-deck pressure–displacement relation
ε	$=Gr^{-1/4}$, used as a small expansion parameter
η	transformed transverse coordinate
θ	dimensionless temperature
κ	$=(T_0-T_\infty)/(T_w-T_\infty)$, jump in wall temperature for discontinuous wall temperature boundary condition
λ	$=U_B'(0)$, wall shear stress for the jet-like boundary layer at $x=0$
μ	$=\theta_B'(0)$, wall heat flux for the jet-like boundary layer at $x=0$
ν	kinematic viscosity
ξ	axial coordinate measured from leading edge of protrusion
ρ	density
τ	shear stress
ω	Fourier transform variable.

not affect the leading order velocity field. In this paper, we demonstrate that although temperature plays a passive role in the double-deck interaction, the presence of the protrusion produces significant local changes in the temperature and heat transfer rates.

The physical model is shown in Fig. 1. We consider steady, laminar natural convection flow along a vertical plate with a small protrusion embedded within the lower deck of the double-deck structure. The plate is assumed to be maintained at a uniform temperature, T_w, which is higher than the ambient temperature T_∞. Two thermal boundary conditions are considered for the protrusion. In the first case, the surface of the protrusion is maintained at the same temperature T_w as the plate. In the second case, the surface of the protrusion is held at a different temperature T_0. The asymptotic structure of the temperature field is different for these two cases. To leading order, the flow is not influenced by temperature perturbations on the double-deck scale. Thus, the flow structure is the same for both cases. The double-deck flow is discussed in Section 2.1. The details of the temperature field for the uniform wall temperature boundary condition and the discontinuous wall temperature boundary condition are considered separately in Sections 2.2 and 2.3 respectively.

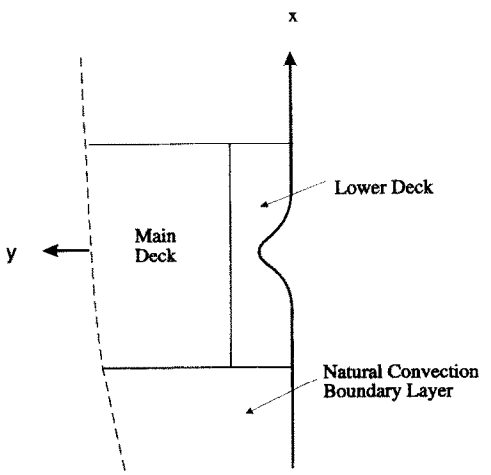

FIG. 1. Physical model and coordinates.

In Sections 2.1, 2.2 and 2.3, the dependence of the double-deck structure on the natural convection boundary layer has been scaled out. The solutions presented in this paper are valid for any jet-like boundary layer flow over a hump. Applying these solutions to other jet-like flows requires a knowledge of the wall shear stress, λ, at the location of the hump for the jet-like flow on the plate, the local displacement effect, γ, of the jet-like flow and the wall heat flux, μ, at the location of the hump for the jet-like flow. Numerical results for the natural convection boundary layer on a vertical plate are provided in detail as an example in Section 4.

The lower deck equations have been solved numerically by a hybrid spectral finite difference method. Details of the numerical method are given in Section 3. Results for a natural convection boundary layer are presented in Section 4 for two Prandtl numbers: $Pr = 0.7$ (air) and $Pr = 8$ (water). A quartic hump has been chosen as a specific example of a protrusion. Since the protrusions considered in this study are very small, we do not expect the results to vary significantly if the shape of the protrusion is changed.

The results indicate that the local wall shear stress and wall heat transfer rates increase on the windward side of the protrusion and decrease on the leeward side for both the uniform wall temperature and discontinuous wall temperature boundary conditions. Results for the total heat transfer rate from the surface of the protrusion have been obtained for various hump heights. For the uniform wall temperature boundary condition, it is found that as the height, h, of the protrusion increases, the total heat transfer rate from its surface increases to a maximum around $h = 1.5$ and then decreases. The total heat transfer rate from the protrusion for the discontinuous wall temperature boundary condition shows a similar trend. The results for $Pr = 8$ (water), however, indicate that for the discontinuous wall temperature boundary condition, the total heat transfer rate reaches a local minimum around $h = 2.25$ and then increases as h is increased further. This increase in heat transfer rate may be attributed to the mixing of cold fluid with hot fluid induced by the recirculation of fluid in the separation bubble. Since the current model is valid only for small-scale separation, the significance of the heat transfer enhancement due to the mixing induced by flow separation cannot be fully elucidated. The results, however, clearly indicate the trend.

2. ANALYSIS

We consider steady, laminar, two-dimensional free convection flow along a vertical flat plate with a small protrusion located at a distance L from its leading edge (Fig. 1). Cartesian coordinates $(\bar{x}, \bar{y})$ are chosen such that the $\bar{x}$-axis is aligned with the direction of gravity, and the $\bar{y}$-axis is normal to the plate. The corresponding velocity components are $(\bar{u}, \bar{v})$. The leading edge is at $\bar{x} = -L$, and the plate is at $\bar{y} = 0$. We introduce the following dimensionless variables:

$$x = \frac{\bar{x}}{L}, \quad y = \frac{\bar{y}}{L} \quad \text{(coordinates)} \tag{1a}$$

$$u = \frac{\bar{u}}{u_0}, \quad v = \frac{\bar{v}}{u_0} \quad \text{(velocities)} \tag{1b}$$

$$p = \frac{\bar{p} - \bar{p}_\infty}{\rho u_0^2} \quad \text{(pressure)} \tag{1c}$$

$$\theta = \frac{T - T_\infty}{T_w - T_\infty} \quad \text{(temperature)}, \tag{1d}$$

where

$$u_0 = \sqrt{(g\beta L(T_w - T_\infty))} \tag{1e}$$

is a reference velocity, g is the gravitational acceleration, β is the thermal expansivity, T_w is the temperature of the plate, T_∞ is the ambient temperature, $\bar{p}_\infty$ is the ambient pressure and ρ is the reference density.

The equations describing the flow are the continuity, Navier–Stokes and energy equations. Employing the Boussinesq approximation, these equations may be written in dimensionless form as

$$\frac{\partial u}{\partial x} + \frac{\partial v}{\partial y} = 0 \tag{2a}$$

$$u\frac{\partial u}{\partial x} + v\frac{\partial u}{\partial y} = -\frac{\partial p}{\partial x} + \theta + \varepsilon^2\left(\frac{\partial^2 u}{\partial x^2} + \frac{\partial^2 u}{\partial y^2}\right) \tag{2b}$$

$$u\frac{\partial v}{\partial x} + v\frac{\partial v}{\partial y} = -\frac{\partial p}{\partial y} + \varepsilon^2\left(\frac{\partial^2 v}{\partial x^2} + \frac{\partial^2 v}{\partial y^2}\right) \tag{2c}$$

$$u\frac{\partial \theta}{\partial x} + v\frac{\partial \theta}{\partial y} = \frac{\varepsilon^2}{Pr}\left(\frac{\partial^2 \theta}{\partial x^2} + \frac{\partial^2 \theta}{\partial y^2}\right), \tag{2d}$$

where

$$\varepsilon = Gr^{-1/4} \tag{2e}$$

is the order of the free convection boundary layer thickness for fluids with Prandtl number of order one,

$$Gr = g\beta(T_w - T_\infty)L^3/\nu^2 \tag{2f}$$

is the Grashof number,

$$Pr = \nu/\alpha \tag{2g}$$

is the Prandtl number, ν is the kinematic viscosity and α is the thermal diffusivity.

Following Merkin [5], we consider protrusions of height of $O(L\varepsilon^{9/7})$ and length of $O(L\varepsilon^{6/7})$, with profiles

$$y = \varepsilon^{9/7} hF(x/\varepsilon^{6/7}), \tag{3}$$

where the function F is such that $hF(X)$ is of order one or less for all $X = x/\varepsilon^{6/7}$. The protrusion or hump may then be taken as a $O(1)$ disturbance within the lower deck of a double-deck structure. The double-deck flow structure is given in detail in ref. [1] and will be described only briefly here.

2.1. *The double deck*

In the main deck or outer layer, the $O(1)$ coordinates are

$$X = \frac{x}{\varepsilon^{6/7}}$$

$$Y = \frac{y}{\varepsilon}. \tag{4}$$

The dependent variables are expanded as

$$u = U_B(Y) + \varepsilon^{2/7} U_1(X, Y) + \cdots$$

$$u = \varepsilon^{1/7} U_1(X, Y) + \cdots$$
$$v = \varepsilon^{4/7} V_1(X, Y) + \cdots$$
$$p = \varepsilon^{4/7} P_1(X, Y) + \cdots$$
$$\theta = \theta_B(Y) + \varepsilon^{2/7} \hat{\theta}_1(X, Y) + \cdots. \quad (5)$$

where $U_B(Y)$ and $\theta_B(Y)$ are the upstream flat-plate boundary layer velocity and temperature profiles, evaluated at $x = 0$. The leading term in the expansion is the boundary layer solution in the absence of the hump, since this is a small perturbation theory. Substitutions of the expansions (5) into equations (2) gives

$$\frac{\partial U_1}{\partial X} + \frac{\partial V_1}{\partial Y} = 0$$
$$U_B(Y)\frac{\partial U_1}{\partial X} + U_B'(Y) V_1 = 0$$
$$U_B(Y)\frac{\partial V_1}{\partial X} = -\frac{\partial P_1}{\partial Y}$$
$$U_B(Y)\frac{\partial \hat{\theta}_1}{\partial X} + \theta_B'(Y) V_1 = 0. \quad (6)$$

The solution of the above equations may be written as

$$U_1 = U_B'(Y) A(X)$$
$$V_1 = -U_B(Y) A'(X)$$
$$P_1 = -A''(X)\int_Y^\infty [U_B(t)]^2 \, dt$$
$$\hat{\theta}_1 = \theta_B'(Y) A(X), \quad (7)$$

where $A(X)$ is an unknown function to be determined by matching with the inner solution, and the prime denotes a derivative.

The solution given by equations (7) does not satisfy the wall boundary conditions and so a *lower deck* is required close to the solid surface where X and $\tilde{Y} = Y/\varepsilon^{2/7}$ are the $O(1)$ coordinates. The perturbations to the upstream boundary layer solution are no longer small in this region, and the expansions take the form

$$u = \varepsilon^{2/7}\gamma^{1/7}\lambda^{3/7} u_1(x_1, y_1) + \cdots$$
$$v = \varepsilon^{5/7}\gamma^{-1/7}\lambda^{4/7} v_1(x_1, y_1) + \cdots$$
$$p = \varepsilon^{4/7}\gamma^{2/7}\lambda^{6/7} p_1(x_1, y_1) + \cdots, \quad (8)$$

where

$$\lambda = U_B'(0),$$
$$\gamma = \int_0^\infty [U_B(t)]^2 \, dt \quad (9)$$

and

$$x_1 = \gamma^{3/7}\lambda^{5/7} X$$
$$y_1 = \gamma^{-1/7}\lambda^{4/7}\varepsilon^{-2/7} Y \quad (10)$$

are scaled coordinates defined for convenience. We also define

$$a(x_1) = \gamma^{-1/7}\lambda^{4/7} A(X) \quad (11)$$

and

$$f(x_1) = \gamma^{-1/7}\lambda^{4/7} F(X). \quad (12)$$

Here, λ is the wall shear stress for the natural convection boundary layer at $x = 0$ in the absence of the hump, and γ is a constant used in the double-deck pressure–displacement relation. The advantage of scaling out λ and γ is that the results for the lower deck velocity and temperature fields in the scaled coordinates are independent of the upstream flat-plate boundary layer solution. The results can therefore be applied to any jet-like boundary flow if the constants λ and γ are known. The asymptotic structure of the temperature field in the lower deck depends on the thermal boundary conditions on the surface of the protrusion and will be considered separately in Sections 2.2 and 2.3. As shown in ref. [1], temperature gradients play only a passive role in the double-deck structure, to leading order. Thus, the leading order velocity and temperature fields are decoupled, and a solution for the velocity field may be obtained without solving the energy equation. The leading order equations in the lower deck are

$$\frac{\partial u_1}{\partial x_1} + \frac{\partial v_1}{\partial y_1} = 0$$
$$u_1\frac{\partial u_1}{\partial x_1} + v_1\frac{\partial u_1}{\partial y_1} = -\frac{\partial p_1}{\partial x_1} + \frac{\partial^2 u_1}{\partial y_1^2}$$
$$\frac{\partial p_1}{\partial y_1} = 0. \quad (13)$$

The expansions (8) must match with the boundary layer solution upstream. Thus,

$$u_1 \to y_1, v_1, p_1 \to 0 \quad \text{as} \quad x_1 \to -\infty. \quad (14)$$

As $y_1 \to \infty$, they must also match with the main deck so that

$$u_1 \to y_1 + a(x_1) \quad \text{as} \quad y_1 \to \infty. \quad (15)$$

On the surface of the protrusion, the no-slip and kinematic boundary conditions must hold. Thus,

$$u_1 = v_1 = 0 \quad \text{on} \quad y_1 = hf(x_1). \quad (16)$$

Finally, since the normal pressure gradient vanishes across the lower deck,

$$p_1 = -\frac{d^2 a}{dx_1^2}, \quad (17)$$

which gives a relation between pressure and displacement.

We now introduce the following transformations:

$$z_1 = y_1 - hf(x_1)$$
$$w_1 = v_1 - hu_1\frac{df}{dx_1}$$
$$d = a(x_1) + hf(x_1). \quad (18)$$

By Prandtl's transposition theorem [10, 11], equations (13) remain unchanged in form under this trans-

formation, with z_1 and w_1 replacing y_1 and v_1 respectively. The boundary conditions become

$$u_1 = w_1 = 0 \quad \text{on} \quad z_1 = 0$$
$$u_1 \to z_1 + d(x_1) \quad \text{as} \quad z_1 \to \infty$$
$$u_1 \to z_1, w_1, p_1 \to 0 \quad \text{as} \quad x_1 \to -\infty. \tag{19}$$

The transformation maps the surface $y_1 = hf(x_1)$ to the flat surface $z_1 = 0$. The transformed coordinates (x_1, z_1) are not orthogonal. However, a regular rectangular computational grid may be used to solve the equations numerically.

2.2. *The thermal boundary layer for uniform wall temperature boundary conditions*

If the surface of the protrusion is maintained at the same temperature, T_w, as the plate, the asymptotic expansion for temperature in the lower deck is given by

$$\theta = 1 + \varepsilon^{2/7}\gamma^{1/7}\lambda^{-4/7}\mu\theta_1(x_1, y_1) + \cdots, \tag{20}$$

where

$$\mu = \theta'_B(0) \tag{21}$$

is the wall heat flux for the natural convection boundary layer for the flat plate at $x = 0$.

The leading order energy equation in the lower deck takes the form

$$u_1 \frac{\partial\theta_1}{\partial x_1} + w_1 \frac{\partial\theta_1}{\partial z_1} = \frac{1}{Pr}\frac{\partial^2\theta_1}{\partial z_1^2}, \tag{22}$$

where the transformation (18) has been used. Equation (22) has to be solved subject to the boundary conditions:

$$\text{at } z_1 = 0, \quad \theta_1 = 0$$
$$\text{as } z_1 \to \infty, \quad \theta_1 \to z_1 + d(x_1)$$
$$\text{as } x_1 \to -\infty, \quad \theta_1 \to z_1. \tag{23}$$

2.3. *The thermal boundary layer for discontinuous wall temperature boundary conditions*

In this section, we consider the case where the surface of the protrusion is held at a temperature T_0 different from T_w. The asymptotic expansion for temperature now takes the form

$$\theta = 1 + (\kappa - 1)\theta_0(x_1, y_1) + \cdots, \tag{24}$$

where

$$\kappa = \frac{T_0 - T_\infty}{T_w - T_\infty} \tag{25}$$

is a dimensionless parameter representing the jump in wall temperature. The leading order energy equation in Prandtl's coordinates is given by

$$u_1 \frac{\partial\theta_0}{\partial x_1} + w_1 \frac{\partial\theta_0}{\partial z_1} = \frac{1}{Pr}\frac{\partial^2\theta_0}{\partial z_1^2}. \tag{26}$$

Matching with the upstream solution yields

$$\theta_0 \to 0 \quad \text{as} \quad x_1 \to -\infty. \tag{27}$$

Matching with the main deck results in

$$\theta_0 \to 0 \quad \text{as} \quad z_1 \to \infty. \tag{28}$$

The wall boundary condition becomes:

$$\text{at } z = 0, \quad \theta_0 = \begin{cases} 1, & x_L < x_1 < x_T \\ 0, & \text{otherwise} \end{cases} \tag{29}$$

where x_L and x_T represent the leading and trailing edges of the hump; that is, $f(x_1) = 0$ if $x_1 < x_L$ or if $x_1 > x_T$.

Equations (26)–(29) imply that $\theta_0 = 0$ if $x_1 < x_L$. Thus, in this case, there is no upstream influence on the double-deck scale. The temperature profile ahead of a discontinuity in wall temperature is influenced only in a small region where streamwise conduction of heat is as important as transverse conduction [1, 12]. This is the region where x and y are of $O(\varepsilon^{3/2})$ and is not considered in this paper.

Since there is no upstream influence, the computations can be started at $x_1 = x_L$. The leading edge singularity is removed by the following transformation:

$$\xi = x_1 - x_L$$
$$\eta = \frac{z_1}{\xi^{1/3}}. \tag{30}$$

In (ξ, η) coordinates, the lower deck energy equation has the form

$$\xi^{2/3}u_1\frac{\partial\theta_0}{\partial\xi} + \left(\xi^{1/3}w_1 - \frac{\eta u_1}{3\xi^{1/3}}\right)\frac{\partial\theta_0}{\partial\eta} = \frac{1}{Pr}\frac{\partial^2\theta_0}{\partial\eta^2}. \tag{31}$$

The boundary conditions are:

$$\text{at } \eta = 0, \quad \theta_0 = \begin{cases} 1, & 0 \leqslant \xi \leqslant (x_T - x_L) \\ 0, & \xi > (x_T - x_L) \end{cases};$$
$$\text{as } \eta \to \infty, \quad \theta_0 = 0. \tag{32}$$

At $\xi = 0$, equation (31) reduces to

$$\frac{\partial^2\theta_0}{\partial\eta^2} + \frac{\tau_0 Pr}{3}\eta^2\frac{\partial\theta_0}{\partial\eta} = 0, \tag{33}$$

where τ_0 is the wall shear stress at $\xi = 0$. The initial conditions for equation (31) are generated by solving equation (33) subject to boundary conditions (32).

3. THE NUMERICAL METHOD

The lower deck momentum equation was solved by a hybrid spectral finite difference method. The numerical method is based on that of Burggraf and Duck [13]. The semi-infinite interval $0 \leqslant z_1 < \infty$ is mapped to a finite interval by the transformation

$$z_1 = G_1(t). \tag{34}$$

The pressure gradient term is eliminated from the momentum equation by differentiating it with respect

to z_1, and the solution variables are split into two components, namely, that corresponding to uniform shear ($u_1 = z_1$) and a perturbation component. The perturbation components are then transformed from physical to spectral variables using the Fourier integral transform in x_1, e.g.

$$\tilde{\tau}^*(\omega, t) = \int_{-\infty}^{\infty} \tilde{\tau}(x_1, t)\, e^{-i\omega x_1}\, dx_1, \tag{35}$$

where the tilde denotes perturbation components and the asterisk denotes a transformed variable. The resulting transport equation for the perturbation shear stress is given by

$$\frac{1}{[G'(t)]^2}\frac{\partial^2\tilde{\tau}^*}{\partial t^2} - \frac{G''(t)}{[G'(t)]^3}\frac{\partial\tilde{\tau}^*}{\partial t} - i\omega G(t)\tilde{\tau}^* = R^*, \tag{36}$$

where

$$R = \tilde{u}_1\frac{\partial\tilde{\tau}}{\partial x_1} + \frac{w_1}{G'(t)}\frac{\partial\tilde{\tau}}{\partial t} \tag{37}$$

and

$$\tilde{\tau} = \frac{1}{G'(t)}\frac{\partial\tilde{u}_1}{\partial t}. \tag{38}$$

The boundary conditions applied to equation (36) are:

$$\text{at } t = 0,$$

$$\frac{\partial\tilde{\tau}^*}{\partial t} = -i\omega^3 G'(t)\left[hf^*(w) - \int_0^{\infty}\tilde{\tau}^*(\omega, t')\, dt'\right];$$

$$\text{as } t \to t_\infty, \quad \tilde{\tau}^* \to 0. \tag{39}$$

This system of equations was solved by a finite difference method. Central differences were applied on the t-derivatives in equation (36). The t-derivative in the interaction condition in equation (39) was replaced by a three-point backward difference formula. Quadratures were evaluated by the trapezoidal rule.

The function $G(t)$ was taken to be

$$G(t) = \frac{t}{1-t}. \tag{40}$$

Uniform steps $\Delta t = t_\infty/(J-1)$ in t, where J is the number of points in the t-direction, correspond to non-uniform steps Δz_1 in z_1. The transformation (40) has the property that points are concentrated close to the solid boundary $z_1 = 0$.

The grid spacings $\Delta\omega$ and Δx_1 were chosen to satisfy the relation

$$\Delta x_1 \Delta\omega = \frac{2\pi}{K} \tag{41}$$

where K is the number of points in the x_1-direction. The range of x_1 was truncated to

$$-\frac{K}{2}\Delta x_1 \leqslant x_1 \leqslant \left(\frac{K}{2} - 1\right)\Delta x_1$$

while the range of ω was truncated to

$$-\frac{K}{2}\Delta\omega \leqslant \omega \leqslant \left(\frac{K}{2} - 1\right)\Delta\omega.$$

Relation (41) allows fast transformation of variables between physical space and spectral space, using the fast Fourier transform technique of Cooley and Tukey [14]. Aliasing errors in the evaluation of the convolution product R^* were removed by padding or truncation [15].

After several trials, t_∞ was fixed at 0.95 and Δx_1 was set to 0.0625. J and K were taken to be 61 and 512, respectively.

The lower deck energy equation was solved in physical space. This avoids problems associated with poor convergence of the discrete Fourier transform near points of discontinuity in the wall boundary temperature. Derivatives in the normal direction were discretized by central differences, while derivatives in the streamwise direction were approximated by a two-point upwind difference scheme. For flows without separation, the upwind difference scheme is equivalent to a backward difference scheme, and the solution is obtained in a single sweep. For separated flows, several sweeps are required in the streamwise direction.

4. RESULTS AND DISCUSSION

Results have been obtained for the quartic jump

$$f(x_1) = \begin{cases} (1-x_1^2)^2, & |x_1| < 1 \\ 0, & |x_1| > 1 \end{cases} \tag{42}$$

for hump heights $h = 0.1$, 1 and 3, and two Prandtl numbers: $Pr = 0.7$ (air) and $Pr = 8$ (water). Details of the main deck displacement, induced pressure and wall shear stress are presented in Figs. 2–4. A typical streamline plot is shown in Fig. 5 for $h = 3$. Results for the heat transfer rates are presented in Figs. 6–9.

There is a region of upstream influence ahead of the protrusion where the main deck flow decelerates, as indicated in Fig. 2. Consequently, the pressure rises

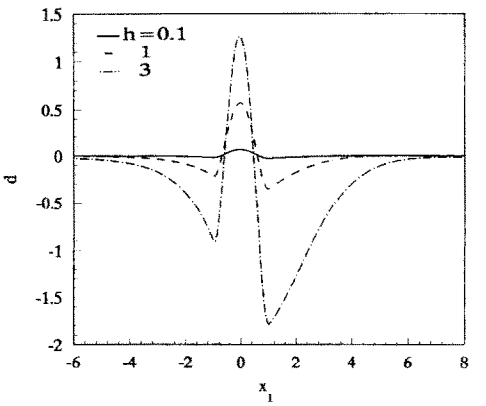

FIG. 2. Main deck displacement.

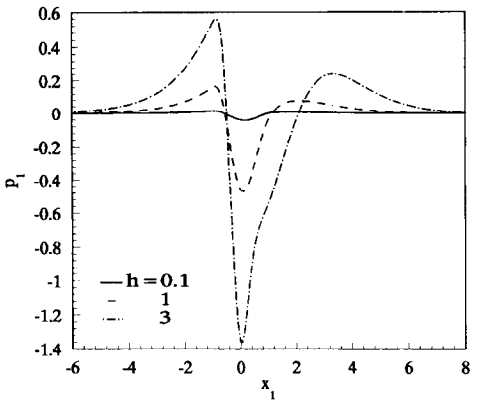

FIG. 3. Pressure distribution.

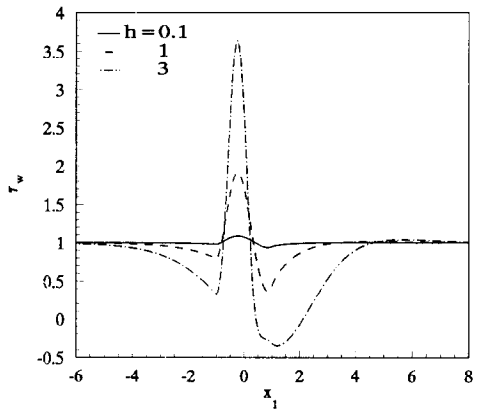

FIG. 4. Wall shear stress distribution.

in this region (Fig. 3), while the wall shear stress decreases (Fig. 4). Beyond the leading edge of the protrusion, the flow accelerates to a maximum near the crest of the protrusion (Fig. 2). As expected, a favorable pressure gradient is developed on the windward side of the hump (Fig. 3), and the wall shear stress rises drastically as the flow accelerates in this region (Fig. 4). On the leeward side of the hump, the flow decelerates rapidly to a minimum at the trailing edge (Fig. 2), and as a result, an adverse pressure gradient is developed (Fig. 3) and the wall shear stress decreases in this region (Fig. 4). The flow separates on the leeward side of the protrusion for hump heights larger than 1.5. Although there is no external free stream in this problem, the upstream natural convection boundary layer acts like a forced flow, leading to flow separation in the wake of the hump. Figure 5 shows the streamlines for separated flow past a

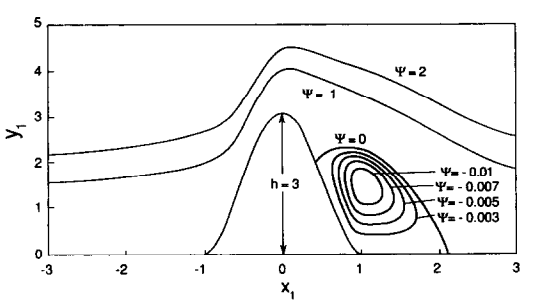

FIG. 5. Streamlines in the lower deck.

protrusion of height $h = 3$. The streamlines above the protrusion are asymmetric due to the displacement effect of the separation bubble in the wake of the protrusion. For $h = 3$, the flow separates around $x_1 = 0.5$ and reattaches at $x_1 = 2.25$, as indicated by Fig. 5. There is a region of negative shear stress inside the separation bubble. Beyond the trailing edge, the flow accelerates again, and the main deck displacement and the wall shear stress approach the unperturbed boundary layer solution asymptotically from below (Figs. 2 and 4). The pressure recovers rapidly in this region and overshoots the ambient value, and then decreases asymptotically to the ambient value from above far downstream of the hump (Fig. 3).

The local Nusselt number for the uniform wall temperature boundary condition, defined in terms of $(T_w - T_\infty)$, the thermal conductivity k, and the length L, can be expressed as

$$Nu = -\varepsilon^{-1}\mu Nu_1 + \cdots, \tag{43}$$

where

$$Nu_1 = \left(\frac{\partial \theta_1}{\partial z_1}\right)_{z_1=0} \tag{44}$$

is the leading term in the asymptotic expansion (43). The variation of $Nu_1(x_1)$ is plotted in Figs. 6(a) and

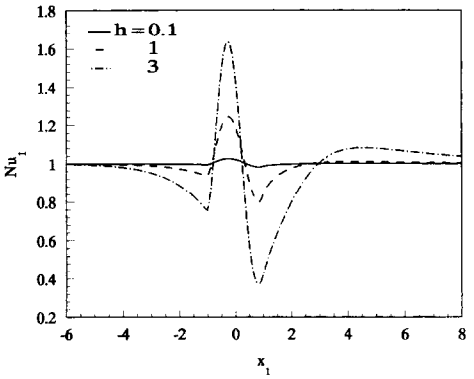

FIG. 6(a). Local heat transfer rate for uniform wall temperature boundary condition and $Pr = 0.7$.

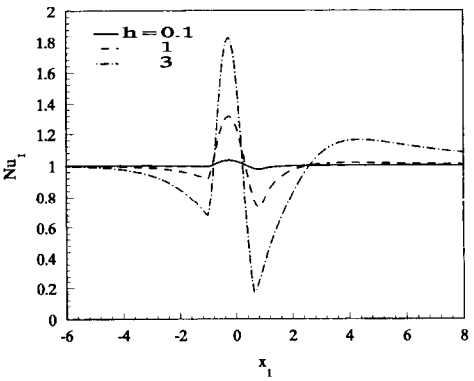

FIG. 6(b). Local heat transfer rate for uniform wall temperature boundary condition and $Pr = 8$.

(b) for $Pr = 0.7$ (air) and $Pr = 8$ (water) respectively. In both cases, the local heat transfer decreases upstream of the protrusion as the flow decelerates, to a minimum at the leading edge of the protrusion. Beyond the leading edge, the wall heat transfer rate rises drastically as the flow accelerates and convects heat away from the plate at a faster rate. The heat transfer rate reaches a maximum slightly ahead of the crest of the hump, and then decreases as the flow decelerates on the leeward side of the hump, to a minimum near the trailing edge. Beyond the trailing edge of the hump, the wall heat transfer rate increases and asymptotically approaches the unperturbed boundary layer solution. For $Pr = 8$, the magnitude of the local heat transfer rates are larger than the corresponding heat transfer rates for $Pr = 0.7$, as the thermal boundary layer is thinner and the temperature gradients at the wall are larger.

The local Nusselt number for the discontinuous wall temperature boundary conditions, defined in terms of $T_w - T_\infty$, the thermal conductivity k and the length L, may be expressed as

$$Nu = \varepsilon^{-9/7}\gamma^{1/7}\lambda^{4/7}Nu_0 + \cdots, \tag{45}$$

where

$$Nu_0 = -\xi^{-1/3}\left(\frac{\partial\theta_0}{\partial\eta}\right)_{\eta=0}. \tag{46}$$

Figure 7(a) shows the variation of $Nu_0(\xi)$ for

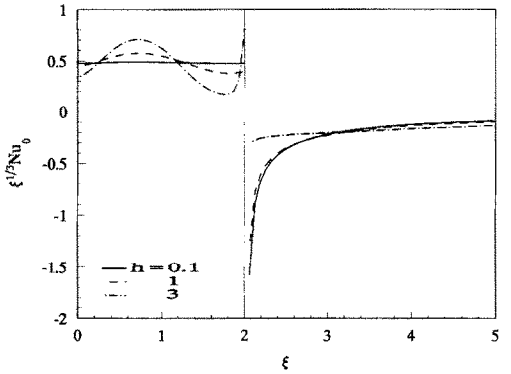

FIG. 7(a). Local heat transfer rate for discontinuous wall temperature boundary condition and $Pr = 0.7$.

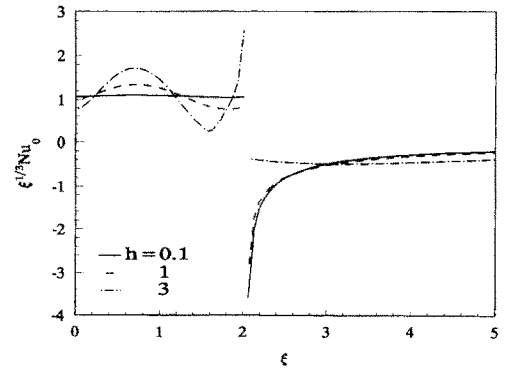

FIG. 7(b). Local heat transfer rate for discontinuous wall temperature boundary condition and $Pr = 8$.

$Pr = 0.7$. Equation (46) indicates that $Nu_0(\xi) \sim \xi^{-1/3}$ near $\xi = 0$. For humps of small height, it is expected that $\xi^{1/3}Nu_0(\xi)$ will be constant along the surface of the hump. Thus, the axial variation of $\xi^{1/3}Nu_0(\xi)$ has been plotted in Fig. 7(a), rather than the variation of $Nu_0(\xi)$. As the height of the protrusion is increased, the flow decelerates ahead of the protrusion and heat is convected away from the surface at a slower rate near the leading edge. The values of $\xi^{1/3}Nu_0(\xi)$ for $h = 1$ and 3 near the leading edge are therefore lower than the corresponding value for $h = 0.1$. The curves for $h = 1$ and 3 show that the local heat transfer rate increases on the windward side of the hump as the flow accelerates, and decreases on the leeward side as the flow decelerates. For $h = 3$, the flow separates ahead of the trailing edge, and the heat transfer rate reaches a local minimum at the separation point, where the local flow is similar to a reverse-stagnation point flow. Just downstream of the separation point, the local wall heat transfer rate rises rapidly as the mixing of cold fluid with hot fluid induced by the recirculating eddy carries heat away from the surface at a faster rate. Downstream of the trailing edge, the wall heat flux changes sign as the hot fluid now transfers heat to the cooler wall. As the thermal boundary layer grows in thickness, the wall heat flux decays asymptotically to zero. The axial variation of $Nu_0(\xi)$ for $Pr = 8$ follows the same trend (Fig. 7(b)). The magnitude of the local heat transfer rates are, however, larger for $Pr = 8$ as the thermal boundary layer is thinner.

The total heat transfer rate, Q, from the surface of the protrusion can be obtained by integrating the local heat transfer rate. For uniform wall temperature boundary conditions, it can be expressed as

$$\frac{Q}{k(T_w - T_\infty)} = -\varepsilon^{-1/7}\gamma^{3/7}\lambda^{5/7}\mu Q_1 + \cdots, \tag{47}$$

where

$$Q_1 = \int_{-1}^{1} Nu_1(x_1)\,dx_1. \tag{48}$$

The values of γ, λ and μ for $Pr = 0.7$ and 8 are given in Table 1. Q_1 is plotted as a function of the hump height h in Fig. 8. It is seen that as h increases, Q_1 increases to a maximum around $h = 1.5$ and then decreases. This may be explained by referring to the local wall heat flux distribution (Figs. 6(a) and (b)). As the height of the protrusion is increased, the local heat transfer rates increase on the windward side of the hump and decrease on the leeward side. For protrusion of heights $h < 1.5$, the net effect is an enhance-

Table 1. Coefficients for heat transfer rate

Pr	γ	λ	μ
0.7	0.3328	0.6789	−0.3532
8.0	0.0601	0.4387	−0.7752

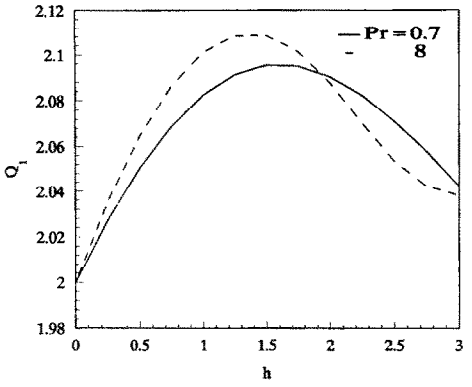

FIG. 8. Total heat transfer rate from surface of protrusion for uniform wall temperature boundary condition.

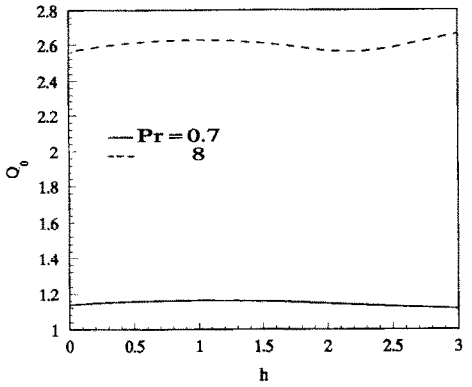

FIG. 9. Total heat transfer rate from surface of protrusion for discontinuous wall temperature boundary condition.

ment in the total heat transfer rate. For humps of larger height, the adverse pressure gradient induced on the leeward side slows down the flow considerably, and as a result, the heat transfer rates decrease. The fluid inside the separation bubble moves very slowly. Heat transfer in this almost stagnant region is mainly by conduction. Locally, the separated region acts like an insulating layer and the heat transfer rates are reduced.

The total heat transfer rate from the surface of the protrusion for the discontinuous wall temperature boundary conditions may be expressed as

$$\frac{Q}{k(T_w - T_\infty)} = \varepsilon^{-3/7}\gamma^{2/7}\lambda^{-1/7}(\kappa - 1)Q_0 + \cdots, \quad (49)$$

where

$$Q_0 = \int_0^2 Nu_0(\xi)\,\mathrm{d}\xi. \quad (50)$$

Figure 9 shows the variation of Q_0 with hump height h. As in the case of the uniform wall temperature boundary condition, Q_0 increases initially with h and then decreases. For $Pr = 8$, Q_0 reaches a local minimum around $h = 2.25$ and then increases again. This increase in the heat transfer rate may be attributed to the mixing of cold fluid with hot fluid induced by the recirculation of fluid in the separation bubble. Since the plate beyond the trailing edge of the protrusion is cooler than the surface of the protrusion, the reverse flow in the separated region brings cooler fluid towards the relatively hotter surface of the protrusion, thereby enhancing the heat transfer rate.

It is worth noting that while the constants γ, λ and μ used in equations (47) and (49) for calculating the total heat transfer rate from the surface of the protrusion depend on the upstream flat-plate boundary layer solution, the values Q_0 and Q_1 presented in Figs. 8 and 9 do not depend on the flat-plate boundary layer solution. Thus, equations (47) and (49) may be used to predict the heat transfer rate from the protrusion for any jet-like boundary layer flow if the values of γ, λ and μ are known.

REFERENCES

1. A. F. Messiter and A. Linan, The vertical plate in laminar free convection: effects of leading and trailing edges and discontinuous temperatures, *J. Appl. Math. Phys. (ZAMP)* **27,** 633–651 (1976).
2. F. T. Smith, A note on a wall jet negotiating a trailing edge, *Q. J. Mech. Appl. Math.* **31,** 473–479 (1978).
3. J. H. Merkin and F. T. Smith, Free convection boundary layers near corners and sharp trailing edge, *J. Appl. Math. Phys. (ZAMP)* **33,** 36–52 (1982).
4. F. T. Smith and P. W. Duck, Separation of jets or thermal boundary layers from a wall, *Q. J. Mech. Appl. Math.* **30,** 143–156 (1977).
5. J. H. Merkin, Free convection boundary layers over humps and indentations, *Q. J. Mech. Appl. Math.* **36,** 71–85 (1983).
6. K. Stewartson and P. G. Williams, Self-induced separation, *Proc. R. Soc. Lond.* **A312,** 181–206 (1969).
7. A. F. Messiter, Boundary layer flow near the trailing edge of a flat plate, *SIAM J. Appl. Math.* **18,** 241–257 (1970).
8. F. T. Smith, Laminar flow over a small hump on a flat plate, *J. Fluid Mech.* **57,** 803–824 (1973).
9. S. Ghosh Moulic and L. S. Yao, Heat transfer near a small heated protrusion on a plate, *Int. J. Heat Mass Transfer* **34,** 1481–1489 (1991).
10. L. Rosenhead (Editor), *Laminar Boundary Layers*. Clarendon Press, Oxford (1963).
11. L. S. Yao, A note on Prandtl's transposition theorem, *J. Heat Transfer* **110,** 507–508 (1988).
12. L. S. Yao, C. L. Tien and S. A. Berger, Thermal analysis of a fast moving slab in two adjacent temperature chambers, *J. Heat Transfer* **98,** 327–329 (1976).
13. O. R. Burggraf and P. W. Duck, Spectral computation of triple-deck flows. In *Numerical and Physical Aspects of Aerodynamic Flows*, pp. 145–148. Springer, Berlin (1981).
14. J. W. Cooley and J. W. Tukey, An algorithm for the machine calculation of complex Fourier series, *Math. Comp.* **19,** 297–301 (1965).
15. C. Canuto, M. Y. Hussaini, A. Quarteroni and T. A. Zang, *Spectral Methods in Fluid Dynamics*. Springer, Berlin (1988).

CONVECTION NATURELLE AUTOUR D'UNE PETITE EXCROISSANCE SUR UNE PLAQUE VERTICALE

Résumé—On considère la convection naturelle au voisinage d'une petite excroissance dans la couche limite d'une plaque plane verticale. Des excroissances de hauteur $\sim L\varepsilon^{9/7}$ et de longueur $\sim L\varepsilon^{6/7}$, où $\varepsilon = Gr^{-1/4}$, sont analysées dans le cadre de la théorie du double pont. Les équations du pont inférieur sont résolues numériquement par une méthode hybride spectrale aux différences finies. Les densités de flux thermiques sont déterminées pour deux conditions aux limites thermiques. Dans le premier cas, l'excroissance est maintenue à la même température que la plaque alors que dans le second cas l'excroissance est à une température plus élevée que celle de la plaque. L'effet de la séparation de la couche limite sur le transfert thermique est étudié.

NATÜRLICHE KONVEKTION IN DER UMGEBUNG EINES KLEINEN VORSPRUNGS AN EINER SENKRECHTEN PLATTE

Zusammenfassung—Betrachtet wird die natürliche Konvektion in der Umgebung eines kleinen Vorsprungs, der in die Grenzschicht einer senkrechten Platte eingebettet ist. Vorsprünge der Höhe $L\varepsilon^{9/7}$ und der Länge $L\varepsilon^{6/7}$ mit $\varepsilon = Gr^{-1/4}$ werden mit Hilfe der Zweischicht-Theorie untersucht. Die Gleichungen für die untere Schicht werden numerisch mit Hilfe einer hybriden spektralen Finite-Differenzen-Methode untersucht. Die Wärmeströme werden für zwei thermische Randbedingungen bestimmt. Im ersten Fall wird der Vorsprung auf gleicher Temperatur wie die Platte gehalten, während im zweiten Fall die Temperatur des Vorsprungs höher liegt als diejenige der Platte. Die Auswirkung einer Grenzschichtablösung auf den Wärmestrom wird untersucht.

ЕСТЕСТВЕННАЯ КОНВЕКЦИЯ ВБЛИЗИ НЕБОЛЬШОГО ВЫСТУПА НА ВЕРТИКАЛЬНОЙ ПЛАСТИНЕ

Аннотация—Исследуется естественная конвекция в пограничном слое вблизи небольшого выступа на вертикальной плоской пластине. Рассматриваются выступы высотой $\sim L\varepsilon^{9/7}$ и длиной $\sim L\varepsilon^{6/7}$, где $\varepsilon = Gr^{-1/4}$. Уравнения решаются численно с использованием гибридного спекторального конечно-разностного метода. Определяются скорости теплопереноса для тепловых граничных условий двух видов. В первом случае температура выступа поддерживается равной температуре пластины, во втором она превышает температуру пластины. Определяется влияние отрыва пограничного слоя на скорость теплопереноса.